A Perturbation-Robust Framework for Admittance Control of Robotic Systems With High-Stiffness Contacts and Heavy Payload

Kangwagye Samuel, *Member, IEEE*, Kevin Haninger, *Member, IEEE*, Roberto Oboe, *Fellow, IEEE*, Sami Haddadin, *Fellow, IEEE*, and Sehoon Oh, *Senior Member, IEEE*

***Abstract*—Applications involving serial manipulators, in both co-manipulation with humans and autonomous operation tasks, require the robot to render high admittance so as to minimize contact forces and maintain stable contacts with high-stiffness surfaces. This can be achieved through admittance control, however, inner loop dynamics limit the bandwidth within which the desired admittance can be rendered from the outer loop. Moreover, perturbations affect the admittance control performance whereas other system specific limitations such as "black box" PD position control in typical industrial manipulators hinder the implementation of more advanced control methods. To address these challenges, a perturbation-robust framework, designed for serial manipulators engaged in contact-rich tasks involving heavy payloads, is introduced in this paper. Within this framework, a generalized Perturbation-Robust Observer (PROB), which exploits the joint velocity measurements and inner loop velocity control model, and accommodates the varying stiffness of contacts through contact force measurements is introduced. Three PROBs including a novel Combined Dynamics Observer (CDYOB) are presented. The CDYOB can render wide-range admittance without bandwidth limitations from the inner loop. Theoretical analyses and experiments with an industrial robot validate the effectiveness of the proposed method.**

***Index Terms*—Compliance and impedance control, force control, Human-Robot Collaboration, motion control.**

Manuscript received 29 January 2024; accepted 13 May 2024. Date of publication 28 May 2024; date of current version 5 June 2024. This letter was recommended for publication by Associate Editor C. Della Santina and Editor J. P. Desai upon evaluation of the reviewers' comments. This work was supported in part by Technology Innovation Program under Grant 20015101 funded by Ministry of Trade, Industry & Energy (MOTIE, Korea), and in part by European Union's Horizon 2020 Research and Innovation Programme under Grant Agreement Number 101058521 – CONVERGING. *(Corresponding author: Sehoon Oh.)*

Kangwagye Samuel is with the Chair of Robotics and Systems Intelligence, Munich Institute of Robotics and Machine Intelligence (MIRMI), Technical University Munich, 80992 Munich, Germany, and also with the Department of Mechanical and Production Engineering, Kyambogo University, Kyambogo, Kampala, Uganda (e-mail: s.kangwagye@tum.de).

Kevin Haninger is with the Department of Automation, Fraunhofer IPK, 10589 Berlin, Germany (e-mail: kevin.haninger@ipk.fraunhofer.de).

Roberto Oboe is with the Department of Management and Engineering, University of Padova, 35122 Vicenza, Italy (e-mail: roberto.oboe@unipd.it).

Sami Haddadin is with the Chair of Robotics and Systems Intelligence, Munich Institute of Robotics and Machine Intelligence (MIRMI), Technical University Munich, 80992 Munich, Germany (e-mail: haddadin@tum.de).

Sehoon Oh is with the Department of Robotics and Mechatronics Engineering, Daegu Gyeongbuk Institute of Science and Technology, Daegu 42988, South Korea (e-mail: sehoon@dgist.ac.kr).

This letter has supplementary downloadable material available at https://doi.org/10.1109/LRA.2024.3406055, provided by the authors.

Digital Object Identifier 10.1109/LRA.2024.3406055

I. Introduction

THE future of robotic manipulators is directed toward an increasingly significant usage in applications that demand interactions with both intricate environments and human counterparts. These applications span a diverse range of tasks, featuring autonomous robot operations such as the autonomous movement of heavy loads in warehouses and the collaborative manipulation of objects and payloads with human intervention. In these scenarios, robots and humans coexist within the same operational space, often in highly dynamic environments with varying contact stiffness. In many applications, high-performance motion control is desired (high accuracy, motion bandwidth, reach and/or payload) as well as contact safety (limited force overshoot, contact stability over a range of stiffnesses). The motion requirements can lead to the use of typical industrial robots, which have a low intrinsic admittance due to their heavy structure and payload. This raises critical concerns regarding the safety of both robots and human collaborators [1].

To ensure safe and effective robot interactions, the concept of impedance/admittance control has played a pivotal role [2]. When admittance control is realized on industrial robots, the control objective is to increase the robot's admittance, with the goal of minimizing contact forces and damping high transient contact forces [3]. Admittance control strategies have been developed to achieve this objective. These include positive velocity feedback inner loop shaping [4], disturbance observer (DOB) approaches, [5], feedforward and PID compensators [3], learning methods [6], neural network techniques [7], among others. However, the general hindrance in these methods is that the range of admittance rendering is limited by the inner loop motion control bandwidth. This is in addition to system-specific limitations such as "black box" position control in typical industrial manipulators.

Furthermore, admittance control performance is affected by disturbances, high-frequency contact forces, and payload force variations. These three factors are collectively called *perturbations* in this paper. Disturbances considered here include nonlinear friction, mechanical vibrations due to higher-order dynamics, and coupling between degrees of freedom (DOF) in task space due to imperfections in joint-level control, as well as external forces acting directly on the joints and links of the robot [8]. High-frequency contact forces arise from the coupling of the robot and the unknown environment dynamics and contact transitions [9]. These may cause higher transient forces and

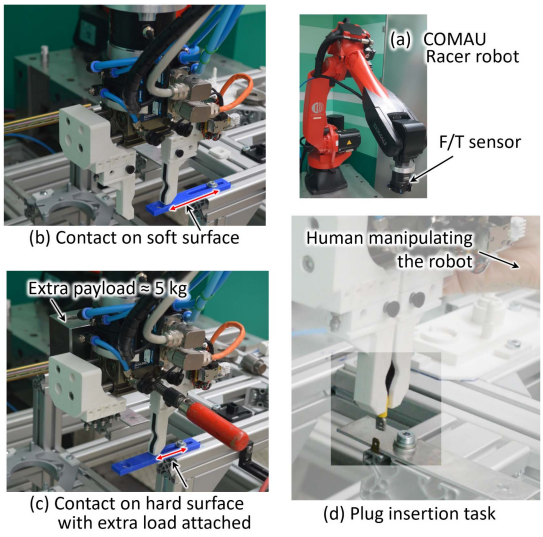

Fig. 1. Illustration of a typical industrial robot involved in autonomous and human assisted operations with contact-rich tasks and payload.

oscillations during contact. Varying forces arising from heavy payloads can amplify low to mid-frequency oscillations. The effects of disturbances and inner loop position control limitations of industrial robots were resolved by realizing the admittance control in task space, with the end-effector force information utilized as feedback in the outer loop [10, §6.4]. However, inner loop dynamics limit the frequency range within which the desired admittance can be rendered in these approaches. Modern control techniques aimed at enhancing admittance rendering accuracy and mitigating contact forces have included sliding mode, advanced feed-forward, and convex synthesis control [11], [12], [13], [14], [15], particularly concerning serial manipulators with accessible inner position control loop.

The motivation of this paper is that inner loop bandwidth limitation and perturbations remain a challenge to realizing stable, high-admittance control. Such limitations are addressed in motion control with Disturbance Observer-based techniques [16], which exploit system models, input/output measurements and loop-shaping to achieve high performance. However, such techniques must be adapted for multi-DOF serial robots with closed inner-loop control, as typical on both collaborative and industrial robots. Furthermore, the controller must be adapted for task-space admittance control, including the end-effector force/torque sensors [17], [18], [19] and payload models [9].

In regard to the above, the main contribution of this paper is the development of a perturbation-robust framework for admittance control in task space of robotic manipulators engaged in contact-rich tasks with heavy payloads. Within this framework, a generalized Perturbation-Robust Observer (PROB) is designed. The PROB accommodates the varying stiffness of contacts through contact force measurements, exploits the command velocity, robot velocity measurements, and inner loop velocity control model to suppress the effects of disturbances, and masks the effect of payload force variations through the robot velocity measurements. The PROB does not require access to the inner velocity control loop but its output modifies the velocity reference signal.

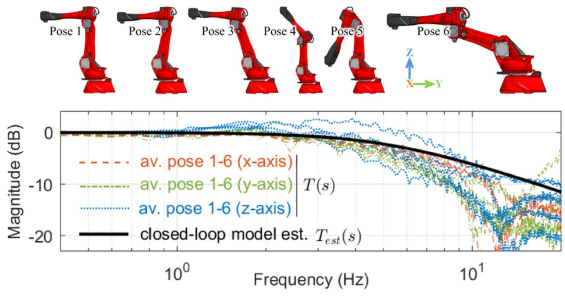

Fig. 2. Closed-loop identification of the position/velocity-controlled manipulator. Top: robot poses. Bottom: magnitude plot of the experimentally measured FRFs and estimated model by curve fitting.

This paper involves design of the three distinct PROBs, including a novel Combined Dynamics Observer (CDYOB), which brings together the dynamic characteristics of inner and outer loops, eliminating the inner loop bandwidth limitation to achieve wide-range admittance rendering from the outer loop. Evolution of the novel CDYOB is introduced by the two previously developed PROBs, i.e., the Task Space Outer-loop Integrated DOB (OIDOBt) in [20] and the Multifunction Observer (MOB) in [21]. The summarized design of OIDOBt and MOB is presented and their strengths and limitations are pointed out to lay a foundation for the CDYOB design. The effectiveness of the proposed method is evaluated through theoretical analyses and experiments.

II. Manipulator Closed Loop Dynamics Identification, Basic Admittance Control, and Problem Description

Consider manipulator tasks that involve low to high-stiffness contact-rich scenarios and heavy payloads. An example studied in this paper is illustrated in Fig. 1. It shows a typical industrial robot in (a) with a "black box" inner position control loop and an outer admittance control loop realized about the robot's Tool Center Point (TCP) by the force/torque (F/T) sensor measurements in task space.

A. Identification of Manipulator Closed Loop Dynamics

Conventional admittance control for robot manipulator has only the admittance model in the outer loop [9]. This has drawbacks such as restricted design freedom and bandwidth limitation by the inner loop dynamics. This paper aims to design a controller outside the inner position control loop of the robot in Fig. 1(a), where a task space model-based approach that includes the nominal inner loop dynamics in its design is suggested.

To this end, the inner closed loop dynamics are measured in task space by closed-loop nonparametric system identification technique. This is motivated by the two advantages of the robot system in Fig. 1(a) of: the availability of command input and measured robot positions/velocities in task space, and, total control is diagonal and each DOF is independent since the Cartesian configuration decouples the joint dynamics. Under position control, a multisine signal is supplied to the robot as the desired position and the corresponding position measurements are recorded. This is conducted on various robot poses, as shown in Fig. 2(top), and the x/y/z-axes of the robot. The obtained data is utilized to compute the actual averaged frequency response

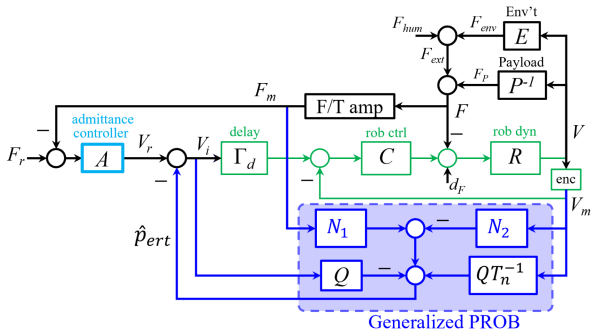

Fig. 3. Generalized admittance control framework showing the proposed perturbation-robust observer for a single DOF. The Laplace operator s is ignored on the subsystems for compactness.

function (FRF) $T(s)$ of all the poses for each axis, as shown in Fig. 2. The estimated FRF, $T_{est}(s)$, is obtained by fitting $T_{est} = \Gamma_d T = \Gamma_d CR/(1+CR)$. Where the dynamics C, R, and Γ_d are actual velocity controller, robot, and time delay, and are given for a single-DOF as

$$C(s) = k_p + \frac{k_i}{s},\ R(s) = \frac{1}{M_r s + B_r},\ \Gamma_d(s) = e^{-t_d s} \quad (1)$$

where k_p and k_i are proportional and integral coefficients, M_r and B_r are robot mass and damping, and t_d is the communication time delay between internal and external controllers. The velocity controller $C(s)$ is modeled as PI and the robot $R(s)$ is modeled as a mass-damper system. The nonlinearities in actual measurements are ignored since they are outside the bandwidth (3–5 Hz) of the robot. The details, including modeling, system identification, and model validation, are presented in [4], [21] by the authors.

B. Basic Admittance Control Framework

Under autonomous operation, the gripper is making contact on soft surface in Fig. 1(b) and hard contact while carrying an extra payload in Fig. 1(c). In manual mode in Fig. 1(d), the human manipulates the robot in the plug insertion task. Here, *perturbations* are defined as follows: During contact, the unknown environment dynamics couple with the robot, potentially causing oscillation or instability, and contact transitions or collisions can also cause higher transient forces. The payload in Fig. 1(c) can generate payload force variations which may lead to oscillations in free space motion or contact. Lastly, the manipulator has disturbances such as nonlinear friction, nonlinearities and coupling between DOFs in task space due to imperfections in joint-level control, gear cogging, and mechanical vibrations due to higher order dynamics.

To this end, Fig. 3 (black solid lines) presents the task space basic admittance control framework of Fig. 1 for a single DOF, which consists of only admittance controller $A(s)$, also called desired admittance, in the outer loop and the manipulator closed loop dynamics (green color). The robot is carrying a heavy payload $P(s)$ and making contacts with a stiff environment $E(s)$. These are modeled as

$$P(s) = 1/M_p s \quad \text{and} \quad E(s) = K_e/s \quad (2)$$

where M_p is payload mass and K_e is environment stiffness.

The generated force F acts on the robot and is measured by the F/T sensor as F_m. The human interacts with the robot through F_{hum} while virtual force can be supplied through F_r to drive the robot autonomously. The desired admittance computes the reference velocity V_r for the inner loop. This framework can be applied to all the robotic manipulators equipped with end effector force and joint position sensors.

C. Problem Description

1) Desired Control Goals and Conditions: The design goal is to achieve broad compliance so as to reduce contact forces and maintain stability during contact with high-stiffness surface. Ideally, it is desired from Fig. 3 that the inner-loop dynamics should be canceled, resulting into rendering the desired admittance through the outer loop, i.e., $\mathcal{V}/\mathcal{F}_{ext} = A$, so that the admittance can be increased without limitation from the actual inner loop dynamics. Assuming that $A(s)$ can be rendered, its gain and transient characteristics determine the level of compliance and speed of response. To this end, $A(s)$ is designed for force input and velocity output as shown below

$$A(s) = 1/(M_a s + B_a) = k_a/(\tau_a s + 1) \quad (3)$$

where M_a is the virtual mass and B_a is the virtual damping, such that $k_a = 1/B_a$ is the gain and $\tau_a = M_a/B_a$ is the time constant. It is desired from (3) to increase k_a and reduce τ_a to achieve high admittance and fast response in the outer loop and realize the overall control goal of safe and effective interactions.

2) Limitations of Basic Framework and Effect of Perturbations and System Specific Limitations: Consider the admittance, $Y = \mathcal{V}/\mathcal{F}_{ext}$, force tracking in autonomous mode, $G = \mathcal{F}/\mathcal{F}_r$, and disturbance, $D = \mathcal{F}/\mathcal{D}_F$, transfer functions for the basic method derived as

$$Y^{\text{basic}} = (C^{-1}T + \Gamma_d T A)/\zeta_1^{\text{basic}} \quad (4)$$

$$G^{\text{basic}} = \Gamma_d T A(P^{-1} + E)/\zeta_2^{\text{basic}} \quad (5)$$

$$D^{\text{basic}} = R/\zeta_2^{\text{basic}} \quad (6)$$

where $\zeta_1^{\text{basic}} = 1 + TC^{-1}P^{-1} + \Gamma_d TAP^{-1}$, $\zeta_2^{\text{basic}} = 1 + C^{-1}T(P^{-1}+E) + \Gamma_d TA(P^{-1}+E)$, and $T = CR/(1+CR)$. The Laplace operator s is ignored from herein after for compactness. Note that, perturbations are described in Fig. 3 as force variations F_{env} and F_p due to environment and payload dynamics, respectively, and the disturbances d_F.

It is observed from (4) that the basic method cannot render the desired admittance since the inner loop, payload, and time delay dynamics cannot be cancelled. These dynamics also affect force tracking performance as shown in (5) and hinder the suppression of the disturbances in (6). The payload forces are not reduced or masked by the basic method and these forces can occur from low to mid-frequency ranges. Moreover, increasing the stiffness of the contacting surface increases peak contact forces [10, §6.3] [22].

Since the outer loop consists only of the admittance controller, the remaining remedy to the above problem is to increase the gain of inner loop velocity controller. Let $k_i = 0$ such that $C = k_p$, making k_p very large, (4)–(6) become

$$Y^{\text{basic}}_{\text{large } k_p} = \Gamma_d A/(1 + \Gamma_d A P^{-1}) \quad (7)$$

$$G^{\text{basic}}_{\text{large } k_p} = \Gamma_d A(P^{-1}+E)/(1+\Gamma_d A(P^{-1}+E)) \quad (8)$$

$$D^{\text{basic}}_{\text{large } k_p} = 0. \quad (9)$$

This result shows that the desired admittance cannot be rendered even after increasing k_p since the payload and time delay dynamics are not canceled as shown in (7). In addition, the high gain does not mask the forces due to environment stiffness as shown in (8). On the other hand, disturbances can be completely suppressed by high gain as shown in (9).

From the above analysis, the design freedom of the basic method is only restricted to adjusting the admittance gain and time constant parameters. However, the inner loop dynamics narrows the bandwidth within which the desired admittance can be rendered from the outer loop. Moreover, increasing the gain to cancel the robot dynamics and disturbances is impossible for systems with specific limitations such as "black box" PD position control of typical industrial robots. To remedy these issues, a generalized robust admittance control method which includes the nominal models of the inner loop dynamics in its design is presented next.

III. Generalized Perturbation-Robust Observer

Fig. 3 (blue lines) presents the generalized Perturbation-Robust Observer (PROB), which is constructed on the basic admittance control framework (black lines), built outside the inner velocity control loop (green lines). The PROB exploits the availability of task space robot velocity and F/T sensor measurements, and the command velocity to estimate the perturbations. The PROB is partly similar to the disturbance observer [16], but has additional inputs through N_1 and N_2, which provide additional design freedom. It can be observed that, there is no need to access the inner loop, instead, the task space velocity reference V_r is modified by $\hat{p}_{ert}$, the output of the PROB. By modifying the velocity reference [3], the proposed approach can be generalized to robotic systems with joint position/velocity and end effector force measurements. Moreover, the proposed PROB framework is inherently robust against model uncertainty as proven for the measured model in Fig. 2 in [20] and [21] for the OIDOBt and MOB methods.

A. Perturbation Estimation With Generalized PROB

From Fig. 3, the estimated perturbation is given by

$$\hat{P}_{ert} = Q[T_n^{-1}\mathcal{V}_m - \mathcal{V}_i] + N_1\mathcal{F}_m - N_2\mathcal{V}_m \quad (10)$$

where $\hat{P}_{ert}$, $\mathcal{V}_\bullet$, and $\mathcal{F}_m$ are the Laplace transforms of $\hat{p}_{ert}$, $V_\bullet$, and F_m, respectively. Q is the Q-filter, T_n is the nominal model of T, N_1 and N_2 are filters to be designed.

The term $T_n^{-1}\mathcal{V}_m - \mathcal{V}_i$ in (10) is designed to robustly estimate the disturbances, d_F, thereby improving the inner-loop motion control accuracy. It possesses the structure of classical DOBs [16], however, the difference is in the design of T_n and the implementation in task space, outside the inner loop. Here, T_n is the nominal model of the closed inner loop dynamics $T = CR/(1+CR)$. Q is the Q-filter, designed as $Q = \omega_Q/(s+\omega_Q)$, where ω_Q is the Q-filter cutoff frequency. Q makes T_n proper and attenuates the measurement noises in V_m and F_m.

The functions of $N_1\mathcal{F}_m$ and $N_2\mathcal{V}_m$ terms are to estimate and suppress the force variations due to contact dynamics and payload, respectively. Where N_1 accommodates the varying stiffness of contacts through contact force measurements and N_2 masks the payload force variations through robot velocity measurements. Detailed designs of N_1 and N_2 is presented in Section III-B.

For utilization in the following sections, the admittance rendering, $Y = \mathcal{V}/\mathcal{F}_{ext}$, force tracking in autonomous robot operation, $G = \mathcal{F}/\mathcal{F}_r$, and force tracking during manual guidance of the robot, $H = \mathcal{F}/\mathcal{F}_{hum}$, transfer functions with the proposed PROB are given below.

$$Y^{\text{PROB}} = [C^{-1}T(1-Q) + \Gamma_d T(A+N_1)]/\zeta_1^{\text{PROB}} \quad (11)$$

$$G^{\text{PROB}} = \Gamma_d TA(P^{-1}+E)/\zeta_2^{\text{PROB}} \quad (12)$$

$$H^{\text{PROB}} = (1-Q+\Gamma_d T(QT_n^{-1}-N_2))/\zeta_2^{\text{PROB}} \quad (13)$$

where $\zeta_1^{\text{PROB}} = (1+TC^{-1}P^{-1})(1-Q)+\Gamma_d T[QT_n^{-1}-N_2+(A+N_1)P^{-1}]$ and $\zeta_2^{\text{PROB}} = [1+C^{-1}T(P^{-1}+E)](1-Q)+\Gamma_d T[QT_n^{-1}-N_2+(A+N_1)(P^{-1}+E)]$.

B. Design of Three Distinct PROBs

In this subsection, PROBs are designed to meet the goal and condition stated in Section II-C1 of canceling the inner loop dynamics to render the desired admittance from the outer loop without bandwidth limitations. This function, and the suppression of the effects of perturbation can be achieved without the need to tune the inner loop gain. To this end, a novel PROB, which eliminates the limitation of the inner loop bandwidth to render the desired admittance from the outer loop is proposed. But before this, a summarized design of the existing two PROBs, i.e., OIDOBt and MOB is presented along with their strengths and limitations to lay a foundation for designing the novel PROB. Therefore, a total of three PROBs are designed with different N_1 and N_2 structures. The design of N_1 and N_2 considers the outer and inner loop dynamic characteristics, i.e., the outer loop admittance controller A and the inner loop dynamics C_n and R_n. Note that, in addition to the requirement of rendering the desired admittance stated in Section II-C1, the design of N_1 and N_2 should also satisfy the design condition of typical DOBs of nominalizing the inner velocity control loop, i.e., make $\mathcal{V}/\mathcal{V}_r|_{Q=1} = T_n$.

1) PROB1. Task Space Outer-Loop Integrated DOB (OIDOBt): The evolution of the PROB design started with the design of OIDOBt in [20] where N_1 and N_2 were designed as follows.

$$N_1^{\text{OIDOBt}} = A(1-Q) \text{ and } N_2^{\text{OIDOBt}} = QAP_n^{-1}. \quad (14)$$

The design in (14) satisfies the $\mathcal{V}/\mathcal{V}_r|_{Q=1} = T_n$ condition. The high-pass filter component, $1-Q$, in N_1 allows the extraction of high-frequency contact forces from the F/T sensor measurements to be suppressed. Therefore, the Q-filter cutoff frequency determines the suppression level of oscillations due to contact dynamics during contact. In N_2, payload is compensated by the inverse of the nominal dynamics with same structure as the actual payload dynamics, i.e., $P_n = 1/M_n s$. In both N_1 and N_2 designs, A converts force into velocity as well as shapes the

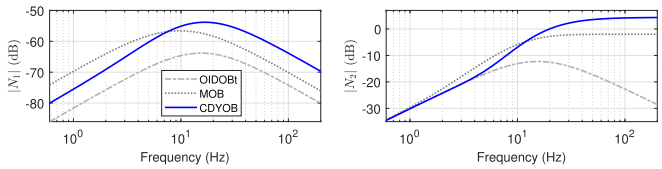

Fig. 4. Plots of $|N_1|$ and $|N_2|$ when $\omega_Q = 15$ Hz.

force information to accurately track the desired admittance in the outer loop.

Note that, the design of N_1 and N_2 in (14) is independent of the actual robot dynamics, thus, the effect of variations in actual dynamics is eliminated. In addition, payload force variations are compensated in all frequency ranges as shown by $|N_2^{\text{OIDOBt}}|$ in Fig. 4.

To check the design condition of rendering the desired admittance, substitute (14) in (11) and set $Q = 1$ to get

$$Y_{Q=1}^{\text{OIDOBt}} = AT_n. \tag{15}$$

It is observed in (15) that, the desired admittance can be rendered only in the low frequency range, i.e., where $|T_n| = 1$. Therefore, the bandwidth of T_n limits the frequency range within which the desired admittance can be rendered. Another limitation of OIDOBt can be observed in (14) that when ω_Q is very large, i.e., $Q = 1$, $N_1^{\text{OIDOBt}} = 0$, implying that, the effects of contact dynamics are suppressed when ω_Q is set as a small value. This is a trade-off with the suppression disturbances, d_F. Moreover, with $\omega_Q = 15$ Hz, $|N_1^{\text{OIDOBt}}|$ is observed to be the lowest in Fig. 4.

2) PROB2. Multi-Function Observer (MOB): To overcome the limitations of OIDOBt, authors proposed the MOB in [21], where N_1 and N_2 were designed as follows.

$$N_1^{\text{MOB}} = QC_n^{-1} \tag{16}$$

$$N_2^{\text{MOB}} = N_2^{\text{OIDOBt}} + QC_n^{-1}P_n^{-1} = Q(A + C_n^{-1})P_n^{-1}. \tag{17}$$

N_1^{MOB} in (16) is designed using nominal velocity controller dynamics, C_n, which takes a different approach from the OIDOBt case in (14). This eliminates the $N_1^{\text{OIDOBt}}|_{Q=1} = 0$ limitation since $N_1^{\text{MOB}}|_{Q=1} \neq 0$, while achieving the function of estimating and suppressing the contact dynamics through C_n^{-1}. Here, C_n^{-1} has a high-pass filter structure and is force input velocity output, thus, it serves the combined purpose of $A(1-Q)$ in OIDOBt. In fact, the MOB suppresses the effects of contact dynamics better than the OIDOBt as shown by its higher $|N_1^{\text{MOB}}|$ in Fig. 4.

On the other hand, N_2^{MOB} is designed from N_2^{OIDOBt} as shown in (17). This is because, designing N_1^{MOB} as QC_n^{-1} necessitates the inclusion of C_n^{-1} in the design of N_2^{MOB} in order to satisfy the $\mathcal{V}/\mathcal{V}_r|_{Q=1} = T_n$ condition. Despite this constraint, payload force variations can be compensated by the MOB in low to mid-frequency ranges as shown by $|N_2^{\text{MOB}}|$ in Fig. 4.

With accurate C_n obtained from a well designed inner loop velocity controller C, the outer loop force tracking accuracy at steady state during contact can be improved. Moreover, ω_Q can be increased to improve disturbance rejection performance while improving contact stability since $N_1^{\text{MOB}} \neq 0$ when $Q = 1$ as with N_1^{OIDOBt}.

Rendering the desired admittance condition is checked by substituting (16) and (17) in (11) and set $Q = 1$ to obtain

$$Y_{Q=1}^{\text{MOB}} = (A + C_n^{-1})T_n. \tag{18}$$

From (18), rendering the desired admittance is affected by the nominal velocity controller even when $|T_n| = 1$. Thus, in addition to the effect of T_n bandwidth as with the OIDOBt, the desired admittance, A, can not be rendered by the MOB due to the presence of C_n^{-1}. Furthermore, due to the utilization of C_n^{-1} in the design of N_1^{MOB} and N_2^{MOB}, a well estimated C_n from a poorly designed C may affect the estimation accuracy of contact dynamics and payload force variations.

3) PROB3. Proposed Combined Dynamics Observer (CDYOB): The design of novel CDYOB combines the inner and outer loop dynamic characteristics to address the limitations of OIDOBt and MOB. To this end, with a constraint that $\mathcal{V}/\mathcal{V}_r|_{Q=1} = T_n$, N_1 and N_2 for CDYOB are designed as shown below

$$N_1^{\text{CDYOB}} = N_1^{\text{MOB}}AR_n^{-1} = QC_n^{-1}AR_n^{-1} \tag{19}$$

$$N_2^{\text{CDYOB}} = N_2^{\text{OIDOBt}}T_n^{-1} = QAP_n^{-1}T_n^{-1}. \tag{20}$$

Substitute (19) and (20) in (11) and set $Q = 1$ to obtain

$$Y_{Q=1}^{\text{CDYOB}} = A. \tag{21}$$

Thus, the goal of rendering the desired admittance has been achieved. Therefore, high gain and fast response characteristics of A in (3) can be realized without any limitation as compared to OIDOBt in (15) and MOB in (17).

The result in (21) is achieved by combining the strengths of OIDOBt and MOB to design N_1^{CDYOB} in (19) and N_2^{CDYOB} in (20). Similar to OIDOBt, the admittance controller A shapes the force information to accurately track the desired admittance in the outer loop as well as converts force into velocity since both $C_n^{-1}R_n^{-1}$ in (19) and $P_n^{-1}T_n^{-1}$ in (20) input and output velocities.

The combination $AC_n^{-1}R_n^{-1}$ in (19) results into a high-pass filter as desired for extracting the high-frequency forces due to contact dynamics. Moreover, since the open loop dynamics, $C_n^{-1}R_n^{-1}$, is an indirect force estimator, more accurate contact dynamics are estimated by the proposed CDYOB. This is shown by $|N_1^{\text{CDYOB}}|$ in Fig. 4 where CDYOB exhibits larger magnitude than OIDOBt and MOB.

In addition to compensating payload forces through P_n^{-1}, the closed loop nominal dynamics T_n^{-1} in (20) accounts for the compensation of the undesired coupling forces between the velocity controlled robot and the attached payload, which are not considered in OIDOBt and MOB. This is validated by the largest $|N_2^{\text{CDYOB}}|$ in Fig. 4 for CDYOB.

To summarize, from its design structure, the proposed novel CDYOB guarantees safety during interactions due to its capability to render the desired admittance from the outer loop without any limitation. Thus, CDYOB is suitable for tasks that involve high speed motion in free space and where the robot and environment dynamics couple such as plug insertions, which require reliable contact stability, as compared to OIDOBt and MOB which have bandwidth limitations of the inner loop.

IV. Further Closed Loop Performance Analysis

A. Parameters Utilized for Analysis

To begin with, the values of parameters in (1) are extracted from T_{est} transfer function in Fig. 2 to get

$$C(s) = 1425 + 38000/s, \quad \Gamma_d(s) = e^{-0.003\,s}, \quad \text{and} \quad R(s) = 1/(41.67s + 1000). \tag{22}$$

Values in (22) are further changed to obtain an FRF with a higher bandwidth, which can be utilized as nominal model C_n and R_n, and the result is given by

$$C_n = 475 + 19000/s, \quad R_n = 1/(16.67s + 600). \tag{23}$$

Furthermore, $A = 1/(8s + 800) = 0.0013/(0.01s + 1)$ following the commonly utilized values by researchers, $K_e = 5 \times 10^5$N/m represents very stiff surfaces, and $M_p = 5$kg, $M_{pn} = 4$kg are used since they are within the payload limits of the robot in Fig. 1 of 7 kg maximum. $\omega_Q = 15$Hz was obtained experimentally with contact control, accounting for both low and high frequency characteristics and the trade-off between latency and noise attenuation.

B. Evaluation of Perturbation Robustness Performance

The perturbations are estimated utilizing end effector force and robot velocity measurements. To this end, re-write (10) to represent component wise the disturbances d_F, contact dynamics in F_m, and payload forces in V_m. To achieve this, derive V_i from Fig. 3 in terms of d_F, F_m, and V_m, substitute the result in (10) and set $Q = 1$ to get

$$\hat{P}_{ert}^{\text{OIDOBt}} = C_n^{-1}D_F - C_n^{-1}\mathcal{F}_m - AP_n^{-1}\mathcal{V}_m \tag{24}$$

$$\hat{P}_{ert}^{\text{MOB}} = C_n^{-1}D_F - P_n^{-1}(A + C_n^{-1})\mathcal{V}_m \tag{25}$$

$$\hat{P}_{ert}^{\text{CDYOB}} = C_n^{-1}D_F + C_n^{-1}(AR_n^{-1} - 1)\mathcal{F}_m - AP_n^{-1}T_n^{-1}\mathcal{V}_m. \tag{26}$$

All the PROBs estimate the disturbances d_F in the same way as shown by the term $C_n^{-1}D_F$. Moreover, $D = \mathcal{F}/\mathcal{D}_F|_{Q=1} = 0$ for all the PROBs, which confirms the disturbance rejection by the $T_n^{-1}\mathcal{V}_m - \mathcal{V}_i$ component in (10) as with classical DOBs [16]. This resolves the limitation by the basic method in (6). On the other hand, the proposed CDYOB leverages its special feature of combining the inner and outer loop dynamics to estimate the high-frequency contact forces and payload force variations, on F_m and V_m components to ensure safety during contact beyond the capabilities of OIDOBt and MOB.

C. Wide-Range Admittance Rendering

The inner loop bandwidth limitation has been eliminated under ideal conditions in (21). Considering the actual case, e.g., when $\omega_Q = 15$ Hz, $|Y|$ is plotted in Fig. 5(top). It can be seen that CDYOB increases the admittance rendering range to almost same as the desired admittance. MOB exhibits resonance due to the effect of C_n in (18) where as the OIDOBt and basic method present same results, being limited by the inner loop dynamics.

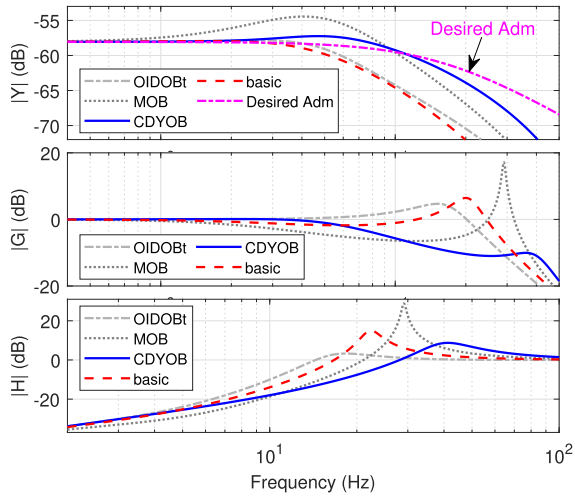

Fig. 5. Plots of $|Y|$ when $\omega_Q = 15$ Hz, and $|G|$, $|H|$ when $Q = 1$.

D. Performance Evaluation of Peak Contact Forces, Force Tracking Accuracy, and Stability During Contact

Let $M_p = M_{pn} = 0$ such that $N_2 = 0$ since payload (gripper) forces are small and overshadowed by contact forces. Substitute N_1 in (12) and (13), and set $Q = 1$ to get

$$G^{\text{OIDOBt}} = AET_n/(1 + AET_n) \tag{27}$$

$$G^{\text{MOB}} = AET_n/(1 + ET_n(A + C_n^{-1})) \tag{28}$$

$$G^{\text{CDYOB}} = AET_n/(1 + AE) \tag{29}$$

$$H^{\text{OIDOBt}} = 1/(1 + AET_n) \tag{30}$$

$$H^{\text{MOB}} = 1/(1 + ET_n(A + C_n^{-1})) \tag{31}$$

$$H^{\text{CDYOB}} = 1/(1 + AE). \tag{32}$$

It can be observed from (27)–(32) that with all the three PROBs, the time delays are eliminated while the velocity controller and robot dynamics are nominalized. This facilitates the increase of k_a and reducing τ_a of the admittance controller without hindrances from the actual dynamics. However, differences are observed in the denominators of each PROB, where the OIDOBt and MOB have T_n, which is absent in CDYOB. This eliminates the bandwidth limitation, thus, gives CDYOB an extra advantage of further increasing the admittance. Furthermore, the magnitudes of (27)–(32) are shown in Fig. 5(bottom), confirming that the CDYOB can improve force tracking accuracy, increase control bandwidth during contact, and reduce resonant forces as compared to basic, ODIOBt, and MOB methods.

Stability during contact is further checked by plotting the poles and zeros of (27)–(29) as shown in Fig. 6. The proposed CDYOB exhibits the best contact stability since all the poles are in the left half plane and far from the neutral axis. All the poles with MOB are stable however, dominant poles are closer to the neutral axis than those of CDYOB. On the other hand, the basic and OIDOBt methods exhibit unstable poles.

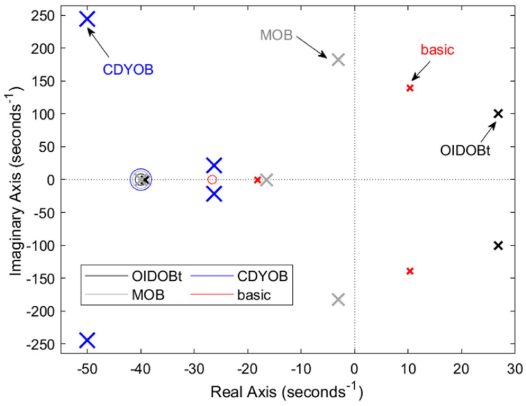

Fig. 6. Pole-zero plot of G when $Q = 1$.

V. Experimental Verification

Experiments involving contact control scenarios with the robot operating autonomously as in Fig. 1(b) and (c) and contact-rich assembly tasks with human assistance in manual mode as in Fig. 1(d) are conducted. The proposed CDYOB is compared with basic, OIDOBt, and MOB methods where performance is evaluated based on peak contact forces and steady-state force tracking error, all of which are desired to be reduced.

The task space position command for implementation on the robot in Fig. 1 is derived from Fig. 3 as

$$\mathcal{X}_i = \Phi_1 \mathcal{F}_r - \Phi_2 \mathcal{F}_m - \Phi_3 \mathcal{V}_m \tag{33}$$

where $\Phi_1 = A/\Phi_4$, $\Phi_2 = (A + N_1)/\Phi_4$, $\Phi_3 = (QT_n^{-1} - N_2)/\Phi_4$, and $\Phi_4 = s(1 - Q)$. The transfer functions Φ_1, Φ_2, and Φ_3 are discretized in MATLAB at a sampling frequency of 1250 Hz on a remote computer, and the result is sent to the robot's internal computer, running in real time, which computes the command signal for the robot controller. $\omega_Q = 15$ Hz was utilized while C_n and R_n were empirically tuned from (23) to get $R_n = 1/(2.5s + 20)$, $C_n = 100 + 400/s$ for OIDOBt and CDYOB, and $C_n = 10 + 400/s$ for MOB.

A. Contact Control

To evaluate suppression of high-frequency contact dynamics, payload force variations, and the effect of variation in the gain and time constant of the desired admittance, three contact control scenarios are considered, i.e., contact on surfaces with varying stiffness, contact with additional payload, and variation in k_a and τ_a.

In all these scenarios, the robot is commanded with a constant virtual force of $F_r = 16$ N to start from a constant position in space, move and collides with the stiff surface and keeps contact. The contacting surface is a 3D printed plastic beam (in blue color) fixed in the robot's workspace as illustrated in Fig. 1(b) and (c). The contact control experiment results for the three conditions are presented in Fig. 7 for the step response time plots and their numerical values of peak contact forces and root mean square values of the force tracking errors at steady state in Fig. 8.

1) Variation in Contact Surface Stiffness: The robot is commanded to make contact on soft and hard surfaces as illustrated by the setup in Fig. 1(b) and (c), respectively, where the distance from the fixture to the contact point (in red) determines the stiffness of the plastic beam. Here, $N_2 = 0$ in (33) since no extra payload is attached to the end effector. Results are presented in Figs. 7 and 8(a), (e), (b), (f) for variation in admittance gain as: for $k_a = 0.0025$: (a) on soft contact and (e) on hard contact, and for $k_a = 0.0013$: (b) on soft contact and (f) on hard contact. Due to increased stiffness, hard surface leads to larger peak contact forces and higher magnitudes of oscillations at steady state for all the methods for similar k_a values. All PROBs show comparable peak contact forces, however, the proposed CDYOB exhibits faster damping after contact and least tracking error, an indication of safe reaction and improved contact stability.

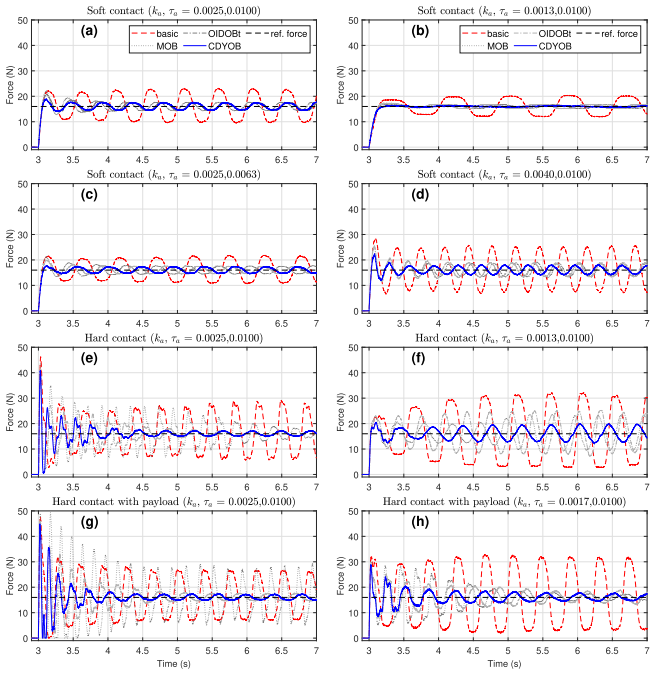

Fig. 7. Experiment results for contact control at various conditions.

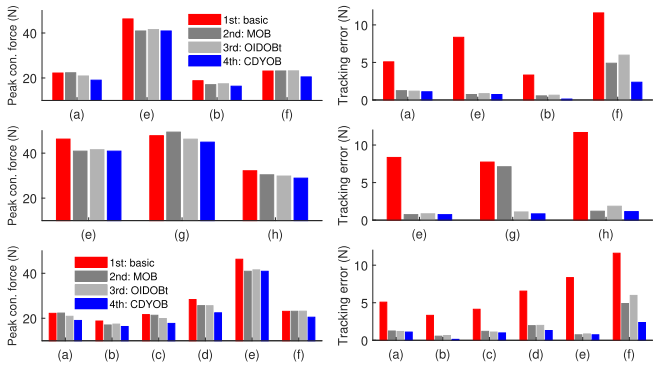

Fig. 8. Peak contact forces and force tracking errors at steady state. Top row: variation in contact stiffness, middle row: variation in payload, and bottom row: effect of admittance controller gain and time constant.

2) Additional Payload: 5 kg payload is added to the end effector as shown in Fig. 1(c) and contact control experiment is repeated on hard contact, with $P_n = 1/5\,s$ for N_2 setting in (33). Results are presented in Figs. 7 and 8(e), (g), (h) for

$k_a = 0.0025$: (e) with no payload and (g) with 5 kg payload attached, and for $k_a = 0.0013$: (h) with 5 kg payload attached. Due to increased momentum by the extra payload, contact forces are larger even for CDYOB (from 40.9 N in (e) to 44.9 N in (g)), however, the CDYOB shows faster damping and there is no big change in the tracking error. On the other hand, other methods' performances deteriorate due to addition of payload.

3) Variation in Gain and Time Constant of Desired Admittance: Results in Figs. 7 and 8(a)–(f) are further studied to examine the influence of k_a and τ_a characteristics of the admittance controller. k_a is varied for (a), (b), and (d) as 0.0025, 0.0013, and 0.004 on soft contact and reduced from 0.025 in (e) to 0.0013 in (f) on hard surface. On soft contact, τ_a is reduced from 0.01 in (a) to 0.0063 in (c). Lowering k_a decreases the robot speed before and on contact, thus contact force is reduced as observed in (a) and (b). The basic method exhibits large oscillations at steady state in (b) while the CDYOB shows no overshoot and tracks the reference with minimal error as compared to OIDOBt and MOB which show larger tracking errors. A small improvement is observed for CDYOB when τ_a is reduced.

To summarize, the proposed CDYOB shows reduced peak contact forces, faster damping, and the least tracking error as compared to basic, OIDOBt, and MOB methods in all the above cases. Therefore, higher admittance can be rendered and the time constant can be reduced to achieve the goal of safe contacts and dynamic interactions. The performance is attributed to the ability of the CDYOB to cancel the effect of robot dynamics, payload, and contact forces while suppressing the effects of perturbations, thus, eliminating the inner loop bandwidth limitation to render the desired admittance as theoretically proven in (21).

B. Actual Demonstrations With Contact-Rich Tasks

The proposed CDYOB, along with basic, OIDOBt, and MOB are utilized for real-world assembly applications with human assistance. Four tasks involving environmental coupling with the robot in Fig. 1(a) are considered: Three tasks with linear motions only by disabling the rotational DOF, i.e., plug insertion with fine positioning, switch insertion onto the rail, peg-in-hole (gear insertion), and one task of colliding the gripper tip with random objects when the rotation 4/5/6 is also activated with CDYOB. In all these tasks, the human manipulates the admittance controlled robot as illustrated in Fig. 1(d) for the plug insertion task. The attached video, also accessible via https://youtu.be/18_bj8L5yU0, shows the demos along with the live plots of x/y/z force responses. The proposed CDYOB is observed to exhibit smallest contact forces, faster damping, and no oscillations during contact.

VI. Conclusion

This paper presented a generalized perturbation-robust framework for admittance control of multi-DOF robotic systems, where a novel CDYOB which overcomes bandwidth limitations by inner position control was developed. While the focus was on robot manipulators, the framework's applicability can be extended to various multi-DOF systems in contact-rich tasks, including mobile manipulations, legged robots, and assistance systems. Future research aims to implement the framework in these contexts and explore enhancements for systems like collaborative robots with accessible inner loop controller parameters.

References

[1] S. Haddadin, A. De Luca, and A. Albu-Schäffer, "Robot collisions: A survey on detection, isolation, and identification," *IEEE Trans. Robot.*, vol. 33, no. 6, pp. 1292–1312, Dec. 2017.

[2] G. Raiola, C. A. Cardenas, T. S. Tadele, T. De Vries, and S. Stramigioli, "Development of a safety-and energy-aware impedance controller for collaborative robots," *IEEE Robot. Automat. Lett.*, vol. 3, no. 2, pp. 1237–1244, Apr. 2018.

[3] A. Q. Keemink, H. van der Kooij, and A. H. Stienen, "Admittance control for physical humanrobot interaction," *Int. J. Robot. Res.*, vol. 37, pp. 1421–1444, Sep. 2018.

[4] K. Samuel, K. Haninger, and S. Oh, "Increasing admittance of industrial robots by velocity feedback inner-loop shaping," in *Proc. IEEE Int. Conf. Robot. Automat.*, 2023, pp. 5228–5234.

[5] M. J. Kim and W. K. Chung, "Disturbance-observer-based PD control of flexible joint robots for asymptotic convergence," *IEEE Trans. Robot.*, vol. 31, no. 6, pp. 1508–1516, Dec. 2015.

[6] X. Yu, P. Liu, W. He, Y. Liu, Q. Chen, and L. Ding, "Human-robot variable impedance skills transfer learning based on dynamic movement primitives," *IEEE Robot. Automat. Lett.*, vol. 7, no. 3, pp. 6463–6470, Jul. 2022.

[7] G. Peng, C. P. Chen, W. He, and C. Yang, "Neural-learning-based force sensorless admittance control for robots with input deadzone," *IEEE Trans. Ind. Electron.*, vol. 68, no. 6, pp. 5184–5196, Jun. 2021.

[8] D. Kaserer, H. Gattringer, and A. Müller, "Time optimal motion planning and admittance control for cooperative grasping," *IEEE Robot. Automat. Lett.*, vol. 5, no. 2, pp. 2216–2223, Apr. 2020.

[9] K. Haninger, M. Radke, A. Vick, and J. Krüger, "Towards high-payload admittance control for manual guidance with environmental contact," *IEEE Robot. Automat. Lett.*, vol. 7, no. 2, pp. 4275–4282, Apr. 2022.

[10] K. Samuel, "Development of advanced robot force control algorithms," Ph.D. dissertation, Daegu Gyeongbuk Institute of Science and Technology, Daegu, South Korea, 2023.

[11] I. Ranatunga, F. L. Lewis, D. O. Popa, and S. M. Tousif, "Adaptive admittance control for human–robot interaction using model reference design and adaptive inverse filtering," *IEEE Trans. control Syst. Technol.*, vol. 25, no. 1, pp. 278–285, Jan. 2017.

[12] E. Sariyildiz, H. Sekiguchi, T. Nozaki, B. Ugurlu, and K. Ohnishi, "A stability analysis for the acceleration-based robust position control of robot manipulators via disturbance observer," *IEEE/ASME Trans. Mechatronics*, vol. 23, no. 5, pp. 2369–2378, Oct. 2018.

[13] R. Kikuuwe, "A sliding-mode-like position controller for admittance control with bounded actuator force," *IEEE/ASME Trans. Mechatronics*, vol. 19, no. 5, pp. 1489–1500, Oct. 2014.

[14] D. Ko, D. Lee, W. K. Chung, and K. Kim, "On the performance and passivity of admittance control with feed-forward input," in *Proc. IEEE/RSJ Int. Conf. Intell. Robots Syst.*, 2022, pp. 11209–11215.

[15] H. Pham and Q. C. Pham, "Convex controller synthesis for robot contact," *IEEE Robot. Automat. Lett.*, vol. 5, no. 2, pp. 3330–3337, Apr. 2020.

[16] S. Li, J. Yang, W. H. Chen, and X. Chen, *Disturbance Observer-Based Control: Methods and Applications*. Boca Raton, FL, USA: CRC Press, 2014.

[17] M. S. Erden and A. Billard, "Hand impedance measurements during interactive manual welding with a robot," *IEEE Trans. Robot.*, vol. 31, no. 1, pp. 168–179, Feb. 2015.

[18] Z. Li, J. Liu, Z. Huang, Y. Peng, H. Pu, and L. Ding, "Adaptive impedance control of human–robot cooperation using reinforcement learning," *IEEE Trans. Ind. Electron.*, vol. 64, no. 10, pp. 8013–8022, Oct. 2017.

[19] M. Bednarczyk, H. Omran, and B. Bayle, "EMG-based variable impedance control with passivity guarantees for collaborative robotics," *IEEE Robot. Automat. Lett.*, vol. 7, no. 2, pp. 4307–4312, Apr. 2022.

[20] K. Samuel, K. Haninger, R. Oboe, and S. Oh, "Task space outer-loop integrated DOB-based admittance control of an industrial robot," *IEEE Trans. Control Syst. Technol.*, vol. 32, no. 3, pp. 974–989, May 2024.

[21] K. Samuel, K. Haninger, R. Oboe, and S. Oh, "Outer-loop admittance and motion control dual improvement via a multi-function observer," *IEEE Trans. Ind. Electron.*, vol. 71, no. 8, pp. 9339–9350, Aug. 2024.

[22] K. Samuel, K. Haninger, and S. Oh, "High-performance admittance control of an industrial robot via disturbance observer," in *Proc. IEEE IECON 48th Annu. Conf. Ind. Electron. Soc.*, 2022, pp. 1–6.